FEDSM-ICNMM2010-' 00%

COMPUTATION OF FLUID FORCES ACTING ON AN INFINITE CYLINDER SUBMITTED TO A SINGLE PHASE CROSS FLOW

André Adobes
EDF R&D Division
6, Quai Watier
78400 Chatou France
andre.adobes@edf.fr

François Jusserand
EDF R&D Division
6, Quai Watier
78400 Chatou France
francois.jusserand@edf.fr

Sofiane Benhamadouche
EDF R&D Division
6, Quai Watier
78400 Chatou France
sofiane.benhamadouche@edf.fr

Yacine Kahil
P&M Curie University - ParisVI
4, Place Jussieu
75252 Paris France
kahil@lmm.jussieu.fr

Salma Belouah
Bordeaux I University
351, Cours de la Libération
33405 Talence France
salma.belouah@gmail.com

ABSTRACT

In Pressurized Water Reactors (PWR), Steam Generator (SG) tubes constitute one of the three barriers which preserve the environment from radioactivity. Excessive tube vibrations under fluid forces, due to the steam-water mixture flow across the tube bundle, can lead to the failure of some tube.

Several methods have been proposed to estimate some upper bounds for these forces. These bounds are applicable at the design stage and are helpful to avoid tube failures. Most of the available methods are based on experimental results that have been obtained on tube bundles installed in scaled test-facilities.

Unlike this popular test-based approach, one combines here Computational Fluid Dynamics (CFD) to High Performance Computing (HPC), in order to estimate fluid forces in a simple case by applying the Direct Numerical Simulation (DNS) method to solve the Navier-Stokes equations.

In the first paragraph, one summarizes the general standard method which allows one to derive the auto-power spectral density of the displacement response at any point of an SG tube, departing from the cross-power spectral densities of fluid forces between any two points along the tube.

In the second paragraph, one recalls the equivalent dimensionless spectrum, which was proposed by Axisa et al. in the early nineties, and which still remains a useful reference in the domain.

One then applies DNS to the test case of a single infinite cylinder, which is submitted to a single phase cross-flow in a rectangular channel. The Reynolds number is equal to 3900.

One presents the time dependent tensors of fluid pressure and viscous stresses, and uses this tensor to estimate the field of non stationary forces that are applied by the fluid, per unit length, at a set of equidistant locations along the tube.

Even if they do still require experimental validations, our computation results are more abundant and detailed than standard experimental results, as well as more flexible to use. They therefore provide an interesting additional source of information. They already allow us to try to get new insights into quantities that would be, in any case, very difficult to obtain experimentally.

Lift, drag, and even the forces acting in the direction of the tube axis, are computed, and can be distinguished one from the other. Fluid forces due to viscous stresses can also be compared to the ones caused by pressure. The degree of correlation of the forces along the tube can also be examined.

INTRODUCTION

In Pressurized Water Reactors (PWR), Steam Generator (SG) tubes isolate the radioactive primary single phase fluid (water), which flows inside the tubes, from the non radioactive secondary two-phase fluid (steam mixed with water), which flows in the SG, outside the tubes. SG tubes therefore constitute

one of the three barriers which preserve the environment from radioactivity.

Cross-flow of the secondary two-phase mixture applies fluid forces onto these tubes and makes them vibrate.

Since excessive vibration can make some tubes crack or even break, methods have been developed, and experiments have been performed for various configurations, in order to calculate tubes vibration levels, and as a result, be able to make sure that sufficient margins exist to avoid any tube failure. A list of major key papers in the domain, which we do not pretend to be exhaustive, is provided in the reference paragraph.

Tube vibrations are mainly governed by fluid forces. These methods, therefore, primarily aim at estimating fluid forces in order to propose an upper bound of them.

Common practice consists in splitting those forces into, forces independent of tube motion on the one hand, and forces that depend on tube motion on the other hand.

In the present paper, we focus on the former. Following many other authors, we consider that the power spectral density of those fluid forces is one of the key points of the problem, and concentrate on its assessment.

Derivation of motion independent fluid forces power spectral density is usually based on an ingenious post-processing of the vibrations measured on tube bundles in scaled test-facilities. Following those methods, one can eventually get a dimensionless envelope power spectral density, which is applicable at the design stage.

Unlike this test based approach, here we try to take advantage of advanced Computational Fluid Dynamics (CFD) combined to High Performance Computing (HPC), and base our methodology on the Direct Numerical Simulation (DNS) solution of Navier-Stockes equations, in the domain occupied by the fluid, which is supposed to be single phase.

STANDARD METHOD FOR COMPUTATION OF AN SG TUBE RESPONSE TO THE EXCITATION BY FLUID FORCES

Let us consider an SG tube submitted to a cross-flow which exerts pressure $p(M', t)$ at time t on point M' of the tube surface, which is denoted by S.

After assuming, (a) the tube can be assimilated to a continuous structure, (b) excitation by the fluid is random, (c) the dynamic response of the tube linearly depends on fluid pressure, one can write [16] :

$$\vec{X}(M, t) = \int_S \left[\int_0^\infty h(M, M', \tau) p(M', t - \tau) \, d\tau \right] \vec{n}(M') \, dS \qquad (1)$$

Where $\vec{X}(M, t)$ denotes the displacement vector of point M of surface S at time t, τ stands for a time interval, $h(M, M', \tau)$ is the impulse response function of the system considered as being linear, and $\vec{n}(M')$ denotes the normal unit vector pointing outward S at point M'.

Equation (1) could be generalized by using the local, time-dependent, whole tensor of fluid stresses $\overline{\overline{\sigma}}(M', t)$, instead of using only the diagonal part of it, which is proportional to scalar pressure $p(M', t)$.

After introducing observation time interval T, one can use relation (2) to define the cross-correlation function $R_{X_{pq}}$ between, (a) $X_p(M_1, t)$ which is the "p" component of displacement vector $\vec{X}$ at point M_1 of surface S and, (b) $X_q(M_2, t)$ which is the "q" component of displacement vector $\vec{X}$ at point M_2 of surface S :

$$R_{X_{pq}}(M_1, M_2, \tau) = \frac{1}{2T} \int_{-T}^{+T} X_p(M_1, t) X_q(M_2, t - \tau) dt \qquad (2)$$

The Fourier transform of time-dependent function $R_{X_{pq}}$, is the frequency dependent cross-power spectral density function between $X_p(M_1, t)$ and $X_q(M_2, t)$. With $j^2 = -1$:

$$S_{X_{pq}}(M_1, M_2, f) = \int_{-\infty}^{+\infty} R_{X_{pq}}(M_1, M_2, \tau) e^{-j2\pi f \tau} d\tau \qquad (3)$$

After inserting expressions (1) and (2) into equation (3), and rearranging, one gets expression (4), where frequency has been omitted for simplicity :

$$S_{X_{pq}}(M_1, M_2) = \\ \iint_{SS} H^*(M_1, M') H(M_2, M'') S_p(M', M'') \vec{n}(M') \vec{n}(M'') dS dS \qquad (4)$$

In equation (4), $H(N, P)$ denotes frequency dependent Fourier transform of the impulse response function between points N and P ; H is also called the transfer function of the linear system ; H^* stands for its transpose conjugate, and $S_p(M', M'', f)$ denotes cross-power spectral density function between pressures at points M' and M''. $S_p(M', M'', f)$ is also the Fourier transform of cross-correlation function $R_p(M', M'', \tau)$ between those two time dependent pressures.

In the particular case where M_1 and M_2 designate the same point M, expression (4) can be readily written :

$$S_{X_{pq}}(M) = \\ \iint_{SS} H^*(M, M') H(M, M'') S_p(M', M'') \vec{n}(M') \vec{n}(M'') dS dS \qquad (5)$$

The above expression shows that, computing a double integral allows one, in principle, to derive displacement

auto-power spectral density function at any point M of an SG tube surface, provided transfer function and pressure cross-power spectral density are known between any two points on the tube surface.

REFERENCE UPPER BOUND SPECTRUM FOR FLUID FORCES ACTING ON SG TUBES IN SINGLE PHASE

All the authors whose papers are quoted in the reference paragraph have indeed strongly contributed to the establishment of nowadays methodology. In the present paper, we shall however only use as a reference, the equivalent dimensionless upper bound spectrum which was proposed by Axisa's in the early nineties, because this spectrum is an attempt to summarize most of the experimental results previously obtained by Axisa and many other authors.

Axisa et al. proposed a test-based method to estimate $S_{F_{pq}}(s',s'',f)$, the cross-power spectral density function between component "p" of force per unit length acting on an SG tube at curvilinear abscissa s', and component "p" of that force at curvilinear abscissa s'' [4].

According to that method, $S_{\bar{F}}(s',s'',f)$ can be derived by applying the following equation :

$$S_{\bar{F}}(s',s'',f) = \left(\frac{1}{2}\bar{\rho}\bar{V}_g^2 D\right)^2 \frac{D}{\bar{V}_g} \exp\left(-\frac{|s''-s'|}{\lambda_c}\right)$$
$$r(s')r(s'')u^2(s')u^2(s'')\frac{L}{\lambda_c}\left[\tilde{\phi}_F\right]_e(f_R) \tag{6}$$

Where :

❑ D denotes tube diameter ;
❑ $\bar{V}_g$ designates the gap velocity, usually defined as :

$$\bar{V}_g = V_\infty \frac{P}{(P-D)} \tag{7}$$

with V_∞, P and D respectively denoting mean velocity upstream the tube bundle, bundle pitch and tube diameter ;

❑ u(s) is defined as :

$$u(s) = \frac{V(s)}{\bar{V}_g} \tag{8}$$

where V(s) stands for secondary fluid velocity at curvilinear abscissa "s",

❑ r(s) is defined as :

$$r(s) = \frac{\rho(s)}{\bar{\rho}} \tag{9}$$

where $\rho(s)$ stands for secondary fluid density at "s" and $\bar{\rho}$ denotes its spatial average over the part of the tube which is submitted to the cross flow.

❑ λ_c is a correlation length which is usually estimated to equal a several tube diameters, and L is a reference length.

❑ $\left[\tilde{\phi}_F\right]_e$ designates an equivalent dimensionless spectrum which depends on reduced frequency f_R :

$$f_R = \frac{fD}{\bar{V}_g} \tag{10}$$

Axisa et al. propose the following envelope for that spectrum :

$$\begin{cases} \left[\tilde{\phi}_F\right]_e(f_R) = 4 \ 10^{-4} f_R^{-0.5} & 0.01 \le f_R \le 0.2 \\ \left[\tilde{\phi}_F\right]_e(f_R) = 3 \ 10^{-6} f_R^{-3.5} & 0.2 \le f_R \le 3 \end{cases} \tag{11}$$

Nowadays, this envelope dimensionless spectrum remains up to date and proves to be very useful to estimate an upper bound of the response of SG tubes to fluid forces in single phase.

Let us now try to readdress the derivation of cross-power spectral density function $S_{\bar{F}}(s',s'',f)$ between forces per unit length exerting at any two points along a tube, in a very simple test-case, at low Reynolds number (3900), by applying the Direct Numerical Simulation (DNS) method.

TEST CASE DESCRIPTION

The test case consists of a horizontal, fixed, rigid, cylindrical tube, submitted to a single phase cross flow in a rectangular channel (figure 1). The different parameters of the test-case are summarized in table 1.
Instantaneous pressure and velocity fields are respectively denoted by p(M,t) and u(M,t). Since the fluid is supposed to be Newtonian, p(M,t) and u(M,t) are supposed to be governed by Navier-Stokes equations [15].

EDF in-house open source CFD tool *Code_Saturne* is used herein (www.code-saturne.org). *Code_Saturne* is an unstructured collocated finite volume solver for incompressible flows using a SIMPLEC algorithm for pressure-velocity coupling, with a Rhie and Chow interpolation to avoid odd-even decoupling on structured meshes. Further details about the code and its capabilities can be found in Archambeau et al. [1].

No subgrid-scale model is used in the present case. In the collocated finite volume approach, all the variables are located

at the centers of gravity of the cells. The momentum equations are solved by considering an explicit mass flux ; the three components of the velocity are thus uncoupled.

A second order centered scheme in space and time is used. It is Crank-Nicolson in time with a linearized convection, and the second order Adams-Bashforth method is used for the part of the diffusion involving the transposed gradient operator, that couples the velocity components.

A centered scheme is used for the convection operator. However, a slope test is used. When the test is positive, 1% upwinding is added to the centered scheme. The non-orthogonalities are taken into account with an implicit reconstruction technique explained in Archambeau et al. [1].

When a non-orthogonal grid is used, the matrix contains only the orthogonal contributions of the different operators. The non-orthogonal part is added to the right hand side of the transport equation. Thus, inner iterations are required for the velocity and pressure equations to make the gradient reconstruction implicit.

D designating tube diameter, the size of the computational domain is *25D × 20D × 4D*. The length of the computational domain upstream the cylinder is equal to *10D*. This is necessary to allow the pressure field to reach an upstream asymptotic behavior.

The mesh refinement is comparable to the one used in previous DNS or LES simulations found in the literature.

The CFL number does not exceed 0.6 during the simulation. The corresponding time step is $\Delta t = 0.005\ D/\ V_\infty$. where V_∞ is the bulk velocity. One flow passage corresponds to 5000 time steps. The computation is performed over more than 20 flow passages. Averaging is then performed in space and time over more than 20 passages. The averaging corresponds to about 100 shedding periods. This should be enough to have a reasonable uncertainty on the statistics

The boundary conditions are detailed in table 2, and table 3 specifies test case modeling features. Table 4 gives basic integral quantities compared to available experimental data from Norberg [18] and Cardell [7], and to DNS data from Kravchenko and Moin [14]. The results are in good agreement concerning these integral quantities. For more recent simulations using DNS or LES with the dynamic model on the present configuration, one can see Kahil et al. [13].
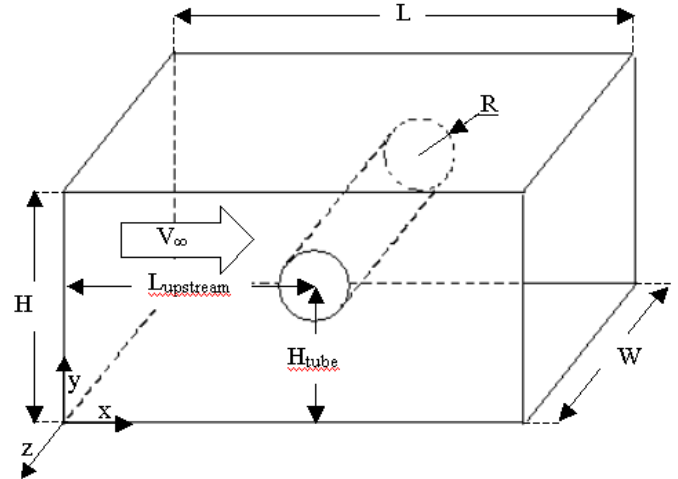

Figure 1 : test case diagram

Table 1 : The parameters of the test-case

Parameter	Value	Unit
Reynolds number Re	3900	-
Upstream velocity V_∞	1	m/s
Fluid density ρ	1	$kg.m^{-3}$
Tube diameter D=2R	1	m
Tube length (spanwise extrusion W)	4	m
Dynamic viscosity μ	1:3900	$kg.m^{-1}.s^{-1}$
Channel length L	25	m
Channel height H	20	m
Tube position $L_{upstream}$	10	m
height H_{tube}	10	m

Table 2 : The boundary conditions

Boundary	Condition
x=0	u(x, y, z, t)=V_∞
x=L	Free outlet
y=0	Symmetry
y=H	Symmetry
z=0	Periodicity
z=W	Periodicity
Tube wall	No slip condition (u=0)

Table 3 : The numerical parameters

Parameter (unit)	Value	Unit
Calculation time step Δt	$5\ 10^{-3}$	s
Corresponding sampling frequency Fs (1:Δt)	200	Hz
Total number of mesh volume cells	$13\ 10^{6}$	-
Number of equal width slices along z axis	256	-
Width of one slice along z (w_s=4:256)	0,015625	m

4   Copyright © 2010 by ASME

Table 4 : Mean integral quantities
compared to experiments and computations

	Present computation	Kravchenko LES [14]	Experiments	
			Norberg [18]	Cardell [7]
$<C_D>$	1.007	1.040	0.98±0.05	-
$<C_L>$	- 0.0005	-	-	-
St	0.208	0.210	-	0.215±0.005

DERIVATION OF FORCES ACTING ON TUBE WALL FROM NON STATIONARY FLUID STRESS TENSOR

Tube wall having been divided along tube axis into 256 cylindrical slices of equal width, let us denote by $\vec{F}_s(t)$ the force per unit length vector applied at time t by the fluid on slice "s". w_s and S_s respectively standing for width and surface of slice "s", $\vec{F}_s(t)$ can be written as :

$$\vec{F}_s(t) = \frac{1}{w_s} \int_{S_s} \overline{\overline{\sigma}}(M,t)\vec{n}(M)dS_s \tag{12}$$

Where $\overline{\overline{\sigma}}(M,t)$ designates the tensor of stresses exerted by the fluid on point M of the tube wall at time t, and $\vec{n}(M)$ is the normal unit vector pointing outward S_s. The fluid being single-phase and Newtonian, $\overline{\overline{\sigma}}(M,t)$ is computed as follows :

$$\overline{\overline{\sigma}}(M,t) = -p(M,t)\overline{\overline{I}} + \mu\left(\overline{\overline{\nabla\vec{u}}}(M,t) + \overline{\overline{\nabla\vec{u}}}(M,t)^t\right) \tag{13}$$

Where $\overline{\overline{I}}$, $\overline{\overline{\nabla\vec{u}}}(M,t)$ and $\overline{\overline{\nabla\vec{u}}}(M,t)^t$ respectively denote the identity tensor, the tensor made of the gradient of vector $\vec{u}(M,t)$, and the transpose of that tensor ; μ stands for dynamic viscosity of the fluid. After inserting equation (13) into equation (12), on obtains the following expression for vector $\vec{F}_s(t)$:

$$\vec{F}_s(t) = \begin{bmatrix} F_s^{Dp}(t) \\ F_s^{Lp}(t) \\ 0 \end{bmatrix} + \begin{bmatrix} F_s^{Dv}(t) \\ F_s^{Lv}(t) \\ F_s^{Av}(t) \end{bmatrix} = \begin{bmatrix} F_s^{D(p+v)}(t) \\ F_s^{L(p+v)}(t) \\ F_s^{A(p+v)}(t) \end{bmatrix} \tag{14}$$

The notations in equation (14) are as follows : capital superscripts "A", "D" and "L" respectively stand for "Axial", "Drag" and "Lift". With our reference axis (figure 1), these three types of force act on the tube wall respectively along the "z", "x" and "y" axis (figure 1). Superscripts "p", "v" and "(p+v)" respectively stand for "pressure", "viscous stresses", and the sum of both. For instance, $F_s^{L(p+v)p}(t)$ denotes lift (superscript "L") per unit length, due to the combined actions of fluid pressure and viscous stresses (superscript "(p+v)") at time t on slice "s".

In the frame of our reference axis, the z component of vector $\vec{n}$ is equal to zero on the whole surface of any slice "s". Tensor $\overline{\overline{I}}$ being diagonal, component $F_s^{Ap}(t)$ of pressure force along the "z" axis is therefore equal to zero.

TIME HISTORIES OF FLUID FORCES

The here above presented DNS method was applied to derive pressure and velocity fields in the fluid domain. Equations (12), (13) and (14) were then used to compute, for each of the 256 slices composing the tube wall, the time histories of the five non zero elements composing vector $\vec{F}_s(t)$.

The beginning of the derived time history vectors was truncated, in order to avoid the transient period which is typically required to make main flow become steady in CFD computations. After truncation of that transient part of time history signals, fifty thousand iterations remained, usable for post-processing purposes. Time step being equal to 5.10^{-3} seconds, the total duration of usable signal was 250 seconds. That period is denoted hereafter by T_o. In order to focus on the fluctuating part of the signals, the derived signals were time-averaged over T_o. For instance, $F_s'^{pL}(t)$, the fluctuating part of the derived component $F_s^{pL}(t)$ was obtained as follows :

$$F_s'^{pL}(t) = F_s^{pL}(t) - \frac{1}{T_o} \int_0^{T_o} F_s^{pL}(t)dt = F_s^{pL}(t) - \left\langle F_s^{pL}(t) \right\rangle_{T_o} \tag{15}$$

Tube having been sub-divided into 256 slices, slices 128 and 129 are the two central slices. From now on, slice 128 is therefore "arbitrarily" chosen as being a reference slice, and most of our results will be presented in reference to it. For illustration of time histories obtained at the end of the whole process, figure 2 and 3 present results obtained on this slice, in time interval [125 s - 150 s].

Figure 2 presents, (a) the fluctuating drag per unit length due to pressure $F_s'^{pD}(t)$, (b) the fluctuating lift per unit length due to pressure $F_s'^{pL}(t)$. Figure 3 presents, (a) the fluctuating drag per unit length due to viscous stresses $F_s'^{vD}(t)$, (b) the fluctuating lift per unit length due to viscous stresses $F_s'^{vL}(t)$.

By observing these two figures, the main conclusions are :

- lift due to pressure seems to be synchronized with lift due to viscous stresses, and the same remark applies to drag ;
- lift due to pressure is much larger than lift due to viscous stresses and the same remark applies to drag ;
- lift due to viscous stresses is more random than lift due to pressure and the same remark applies to drag.
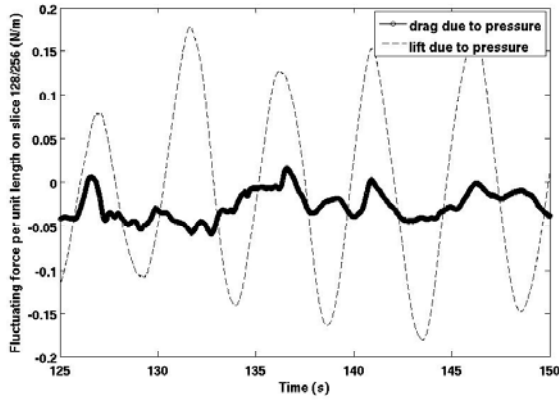- lift is larger than drag both for the pressure and the viscosity term.

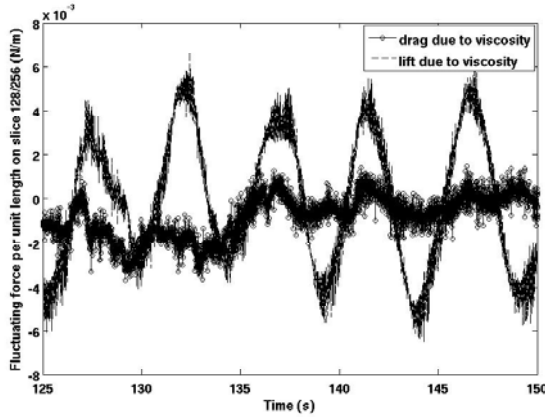Figure 2 : fluctuating forces $F'^{pD}_s(t)$ and $F'^{pL}_s(t)$

Figure 3 : fluctuating forces $F'^{vL}_s(t)$ and $F'^{vD}_s(t)$

The time averages of $F^{pD}_s(t)$, $F^{vL}_s(t)$, $F^{vD}_s(t)$ and $F^{pL}_s(t)$ over time interval [0 s – 250 s] are provided in table 5, which highlights that :

- the two mean drag forces are predominant over the two corresponding mean lift forces,
- either in the drag, or in the lift direction, the pressure term is about 25 times larger than the viscous term.

Table 5 : time-averaged values of drags and lifts at slice 128

Time-average force	Value (N/m)
$\langle F^{pD}_s(t) \rangle_{T_o}$	0,5385
$\langle F^{vD}_s(t) \rangle_{T_o}$	0,0235
$\langle F^{pL}_s(t) \rangle_{T_o}$	0,0029
$\langle F^{vL}_s(t) \rangle_{T_o}$	0,0001

AUTO-POWER SPECTRAL DENSITIES OF FLUID FORCES

The auto-power spectral densities of the five non zero fluctuating forces per unit length were computed for the 256 adjacent slices composing the tube wall, by using "pwelch", an "m-file" available in the frame of MATLAB[©] 7.7.0 [26]. An overlap of 50 % between two consecutive blocks was used ; a Hanning window was used ; zero padding of the last block was necessary since the number of iterations (50000) was not a power of two.

According to Shannon's theorem, sampling frequency "Fs" being equal to 200 Hz, the derived auto-power spectral densities should in principle have been valid up to 100 Hz. On the other hand, frequency resolution of power spectral densities however depends on block length, which is typically a power of two.

Fifty thousand iterations being available in our test-case, block length could attain 32768 points, leading then to a frequency step Δf of the spectra, equal to "6,10 10^{-3} Hz".

The choice of an optimum block length generally results, in practice, from a compromise. A sensitivity analysis of the auto-power spectra densities to the block length was therefore performed. Lift per unit length due to viscous stresses acting on slice 128 was arbitrarily chosen for that analysis.

The derived auto-power spectral densities are plotted versus block length on figure 4, where the number of points composing each block varies from 1024 to 32768. For the smallest block lengths, the peak expected from Karman's vortex street at Strouhal Frequency is difficult to distinguish.

It also gets sharper and sharper with increasing block length.

From the case of the block, made of 16384 points, to the case of the longest block, made of 32678 points, the shape of the peak due to Karman's vortex street does not evolve, and Strouhal number can be estimated at "0,21".

Moreover, for the 32678 point blocks case, some oscillations appear in the curve representing the auto-spectral power density, in the frequency region below that peak.

These oscillations are attributed to excessive zero padding in comparison with real data. We have adopted the block length of 16384 points as a best compromise.

An important point to be observed on figure 4 is that the auto-power spectral density increases above 10 Hz. Such a behavior of a spectrum associated to buffeting forces is considered as being non physical : an artifact in the DNS computation is suspected.

The origin of this artifact, which could be associated with an insufficient refinement of the mesh, is being investigated. The frequency range of validity of the spectra reported in this paper is restricted to [0 - 10 Hz].

For comparisons, it is interesting to superimpose, on the same plot, the auto-power spectral density functions of the fluctuating parts of the five non zero components (see equation 14) which compose vector $\vec{F}_s(t)$:

(a) drags due to pressure and viscous stresses,
(b) lifts due to pressure and viscous stresses,
(c) axial force due to viscous stresses.

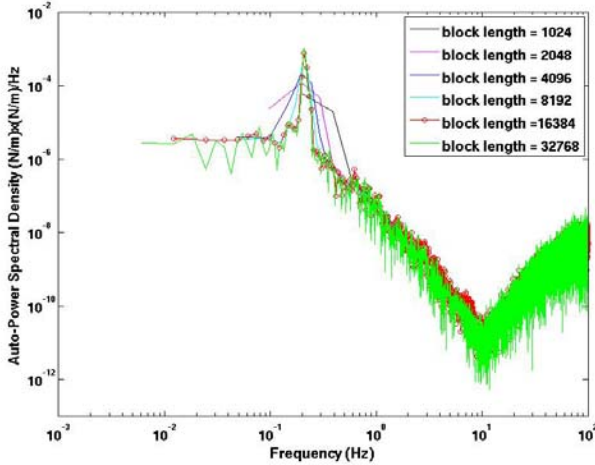This superposition is presented in figure 5 for slice 128.

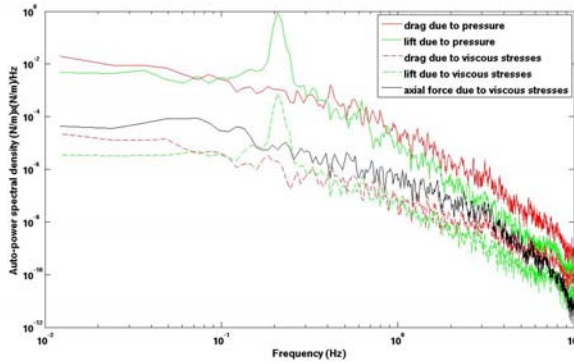Figure 4 : auto-power spectra densities versus block length

Figure 5 : auto-power spectral density functions of the fluctuating parts of the five non zero components of $\vec{F}_s(t)$

Figure 5 confirms the strong predominance of forces due to pressure over forces due to viscous stresses. It highlights the effect of Von Karman's streets on the two kinds of lift (due to pressure and viscous stresses). It suggests that axial forces due to viscous stresses are at least of the same order or magnitude as drag and lift due to viscous stresses. The negative slopes of the five spectra also slightly differ one from another.

On figure 6, the scaled auto-power spectral densities of lift and drag per unit length, both obtained at slice 128 by adding pressure and viscous effects, are presented versus reduced frequency.

Taking into account test-case parameter values (table 1), reduced frequency f_R is derived from frequency f as follows :

$$f_R = \frac{fD}{\overline{V}_g} = \frac{(H-D)}{H} \frac{fD}{V_\infty} = 0{,}95f \qquad (16)$$

In order to compare densities to the dimensionless equivalent envelope spectrum proposed by Axisa et al. (equation 11), both have been scaled in coherence with the length and diameter of a "reference tube" [2] : on the one hand, the ratio between test-case tube diameter (D=1 m), and "reference tube" diameter ($D_{ref} = 2.0 \, 10^{-2} \, m$), and, on the other hand, the ratio between test-case tube length (W=4 m), and "reference tube" length ($L_{ref} = 1m$).

Taking into account test-case parameter values (table 1), scaled auto-power spectral densities of lift and drag $S_{r\vec{F}}(sl, sl, f_R)$ are then derived as follows :

$$S_{r\vec{F}}(sl, sl, f_R) = \frac{1}{\left(\frac{1}{2}\overline{\rho}\overline{V}_g^2 D\right)^2 \frac{D}{\overline{V}_g}} \left(\frac{D_{ref}}{D} \frac{W}{L_{ref}}\right) S_{\vec{F}}(sl, sl, f_R) \qquad (17)$$

$$\approx 0{,}27436 \, S_{\vec{F}}(sl, sl, f_R)$$

The scaled auto-power spectral densities of lift, $S_{rL}(sl, sl, f_R)$, and drag, $S_{rD}(sl, sl, f_R)$, are superimposed on test-based envelope equivalent spectrum proposed by Axisa et al. (equation 11). A linear regression of the curves for scaled lift and drag is performed, in the log-log frame axis, in the reduced frequency range [0,24-3]. This regression suggests a slope of "– 4,27" (dashed red straight line) for lift, and a slope of "– 3,41" (dashed green straight line) for drag. Both slopes define an interval which includes the slope of "-3,5" proposed for the envelope equivalent spectrum.
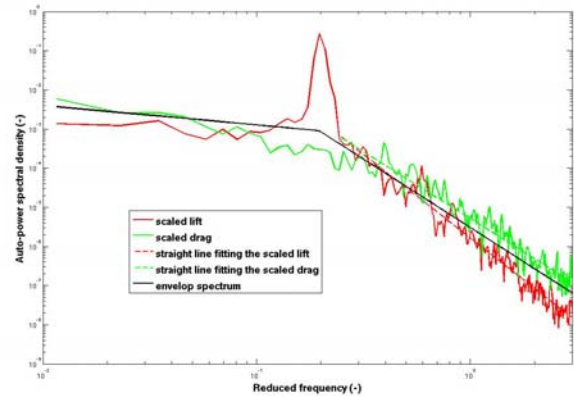

Figure 6 : scaled auto-power spectral densities of lift and drag per unit length versus test-based envelope equivalent spectrum proposed by Axisa et al. (equation 11)

CORRELATION OF FORCES ALONG THE TUBE

Sometimes called coherency squared function, the coherence function $\gamma_{x;y}^2$ is a real-valued frequency dependent function, which characterizes the degree of correlation between two

signals, x and y, defined by their respective time histories, $x(t)$ and $y(t)$ [5]. It satisfies for all f,

$$0 \leq \gamma_{x;y}^2(f) \leq 1 \qquad (18)$$

If $x(t)$ and $y(t)$ are completely unrelated, the coherence function is equal to zero. If the coherence function is greater than zero but less than unity, one or more of the three following possible physical situations exist :

- extraneous noise is present in signal time histories,
- some non linearity exists in the system,
- $y(t)$ is an output due to an input $x(t)$ and to other inputs.

With these elements in mind, we can consider $x(t)$ and $y(t)$ as being two of the five components of force per unit length which build vector $\vec{F}_s(t)$. In order to precisely define the coherence functions that we address, we subscript them with two slice indexes : $s1$ (for x) and $s2$ (for y), and we superscript them with two non zero components of the fluid forces vectors.

For instance, $\gamma^2{}_{s1;s2}^{L(p+v);L(p+v)}$ denotes the coherence function between, the total lift, i.e. the sum of the lift due to pressure plus the lift due to viscous stresses [superscript L(p+v)], computed at slice "s1" on the one hand, and the total lift computed at slice "s2" on the other hand :

$$\gamma^2(f)_{s1;s2}^{L(p+v);L(p+v)} = \frac{\left|S_{L(p+v)}(s1,s2,f)\right|^2}{S_{L(p+v)}(s1,s1,f)\,S_{L(p+v)}(s2,s2,f)} \quad (19)$$

It is common practice to assume the following equation :

$$\gamma^2(f)_{s1;s2}^{L(p+v);L(p+v)} = \exp\left\{-2\frac{|s2-s1|}{\lambda c}\right\} \qquad (20)$$

Where λc denotes correlation length ; λc is generally supposed to be independent of f, and equal to a few tube diameters.
Coherence function defined by equation (19) was computed by using "mscohere", an "m-file" available in the frame of MATLAB© 7.7.0 [26].
In order to ensure consistency, with the power spectral densities computed elsewhere in the paper, Hanning windowing, and an overlap of 50 % between the blocks made of 16384 points, were used again, with zero padding of the last block.
The derived coherence functions were in principle valid up to 100 Hz, but again, due to a likely artifact in DNS

computations, results were considered only in the first tenth of that range : [0-10 Hz].
Figure 7 displays six of the coherence functions obtained, always taking the central slice (n°128) as a reference. These are the coherence functions between, on the one hand, total lift at slice 128, and, on the other hand, total lifts at slices 1, 31, 61, 91, 121 and 128.
Of course, the coherence between the signal at slice 128 and itself equals one on the whole frequency range (black horizontal straight line y=1).
With the exception of that particular curve, the other five curves all seem to be chaotic and no particular trend can be observed.
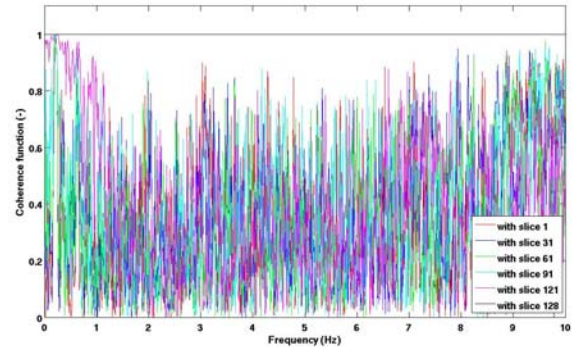

Figure 7 : coherence functions between total lift at slice 128, and total lifts at slices 1, 31, 61, 91, 121 and 128

One conclusion which can be drawn from figure 7, is that our computations do not suggest a coherence function of the exponential type (equation 20). If such a correlation had been proved by our computations, figure 7 would be composed of horizontal straight lines, whose level would have been decreasing with increasing distance between the considered slices and our reference slice (n°128).
In our opinion, coherence function is greater than zero but less than unity, probably at least for the second and third of the three above mentioned possible reasons. The cylinder being rigid and fixed, all information travels through the fluid and no information travels along the tube itself.
For instance, information about total lift per unit length between any two slices along the cylinder (figure 7) exclusively travels through the fluid.
When traveling from one slice to any other slice, information about lift is filtered by at least two non linear operators : firstly, the Navier-Stokes equation itself ; secondly, the combination of the operations in equation 12.
We can however try to get some more insight into the coherence functions by zooming in on figure 7 in the vicinity of Von Karman's vortex street which occurs at 0,21 Hz, e.g. in the frequency range [0-0,5 Hz]. This zoom is displayed in figure 8.
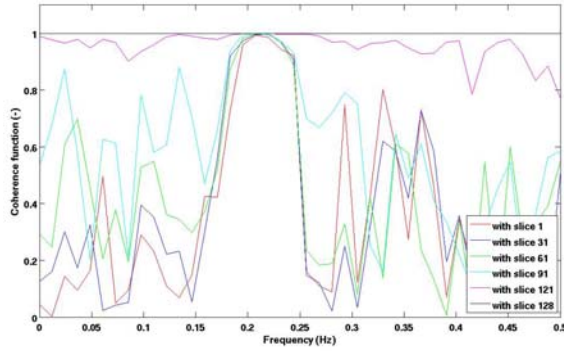
Figure 8 : zoom of figure 7 in the vicinity of Strouhal frequency (0,21 Hz)

Figure 8 teaches us that, coherence function between any slice and the central slice (n°128), is equal to unity in a frequency range of about a tenth of an Hertz around Strouhal frequency.

This means that, even at distances as long as 2 diameters, which is the distance between slice 128 and slice 1, none of the three conditions for reducing coherence function is fulfilled.

After plotting the coherence functions between central slice n°128 and other slices (figures 7 and 8), we now plot all the coherence functions between slice 128 and all the other slices.

Those 128 functions are plotted as a function of the distance between the slices, for various frequencies : figure 9 arbitrarily displays the curves obtained for frequencies "0,0122 Hz", "0,21 Hz", "2.43 Hz", "4.87 Hz", "07,31 Hz", "9,73 Hz".

As could be intuited, one can observe on figure 9 that the two less chaotic curves are precisely the ones that are obtained for the lowest frequencies, namely for 0,0122 Hz and 0,21 Hz. The one corresponding to Strouhal frequency (0,21 Hz) is the most remarkable because it remains nearly equal to unity along the whole tube (see straight green line on top of figure 9).
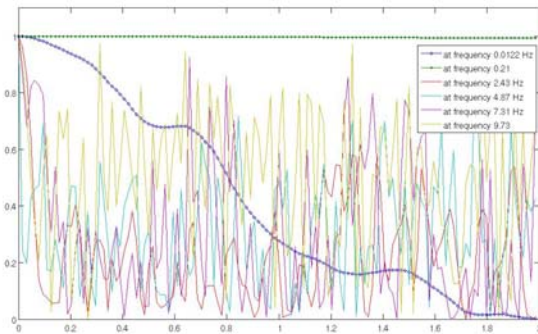

Figure 9 : coherence functions versus distance between slice 128 and all the slices for six arbitrarily chosen frequencies

One also notices that the coherence function which is generally proposed, i.e. $\exp\left\{-2\dfrac{|s2-s1|}{\lambda c}\right\}$, has two derivatives at $(s2=s1)$: $-\dfrac{2}{\lambda c}$ when $(s2>s1)$ and $\dfrac{2}{\lambda c}$ when $(s2<s1)$. It is therefore not differentiable at $(s2=s1)$.

The curve computed for frequency f=0,0122 Hz however suggests (see left starting point of the blue smoothly decreasing curve), that coherence function should on the contrary be differentiable at $(s2=s1)$: blue curve suggest a null derivative at that point for f=0,0122 Hz.

CONCLUSION

Firstly, we recalled the standard method to compute the auto-power spectral density of the displacement of a tube, on the basis of the cross-power spectral density of the fluid forces which are applied along the tube.

Secondly, we recalled Axisa's reference envelope spectrum, which remains very useful to estimate an upper bound of motion independent fluid forces applied to SG tubes in single phase cross-flows.

Application of the DNS method to the test case of a cylinder submitted to a single phase cross-flow at Reynolds number 3900, then allowed us to estimate the non stationary forces that are applied by the fluid, per unit length, at the various locations along the whole tube.

On the basis of the results that have been presented for that test-case, and in expectation of experimental validations that are indeed required, it appears that, in the test-case that we addressed, which is extremely simple compared to the industrial application :
- lift, drag, and even the forces acting in the direction of the tube axis are nowadays computable and distinguishable ;
- fluid forces due to viscous stresses can be compared to the ones caused by pressure ;
- computed spectra fall close to dimensionless envelope spectrum ;
- correlation length is a concept which does not seem to exist in the results of our computations, which lead to chaotic coherence functions, especially, and probably as expected, for higher frequencies ; the exception to this chaotic behavior is the one observed in a tenth of the Hertz frequency band around Strouhal frequency.

In conclusion, CFD seems to be a useful and interesting tool because it reveals quantities that no experiment can provide, even in single phase. For this reason, are CFD results also difficult to validate, at least to such a detailed point ; and this constitutes a challenge for the upcoming experimenters.

EDF's efforts to estimate real fluid forces applied on SG tubes are likely to be continued in the future by considering test cases closer to the industrial concern, as well as more and more performing methods and computational means.

REFERENCES

[1] ARCHAMBEAU, F., MECHITOUA, N., SAKIZ, M., *"Code_Saturne : A Finite Volume Code for the Computation of Turbulent Incompressible Flows"*, Industrial Applications. International Journal on Finite Volumes - Vol. 1, 2004

[2] AU-YANG, M.K., *"Turbulent Buffeting of a Multi-Span Tube Bundle"*, Journal of Vibration, Acoustics, Stress and Reliability in Design, ISSN 0739-3713, Vol. 108, n°2, pp. 150-154, (1986)

[3] AU-YANG, M.K., BLEVINS, R.D., MULCAHY, T.M., *"Flow-Induced Vibration Analysis of Tube Bundles"*, ASME Journal of Pressure Vessel Technology 113, 257–266, (1991)

[4] AXISA, F., ANTUNES, J., VILLARD, B., *"Random Excitation of Heat Exchangers Tubes By Cross-Flow"*, Journal of Fluids and Structures - Vol. 4, 321-341, (1990)

[5] BENDAT, J., S., PIERSOL, A.G., *"Random Data Analysis and Measurement Procedures"*, John Wiley & Sons, 2nd Edition

[6] BLEVINS, R.D., GIBERT, R.J., VILLARD, B., *"Experiments on Vibration of Heat Exchanger Tube Arrays in Cross Flow"*, in Transactions of the 6th International SMIRT Conference, Paper B6/9, (1981)

[7] CARDELL, G., S. *"Flow Past a Circular Cylinder with a Permeable Splitter Plate"*, Ph.D. Thesis, Graduate Aeronautical Laboratory, California Inst. Of Technology (1993)

[8] CHEN, S.S., JENDRZEJCZYK, J.A., *"Fluid Excitation Forces Acting on a Square Tube Array"*, Journal of Fluids Engineering, 109, 415-423

[9] DELANGRE, E., BEAUFILS, B. ANTUNES, J., *"The Numerical Prediction of Vibrations in Tube Bundles Induced by Cross-Flow Turbulence"*, In Proceedings of the Fifth International Conference on Flow-Induced Vibration, pp. 253-260, (1991)

[10] DE LANGRE, E. , VILLARD, B., *"An Upper Bound on Random Buffeting Forces caused by Two-Phase Flows Across Tubes"*, Journal of Fluids and Structures 12, 1005–1023, (1998)

[11] JUSSERAND, F., ADOBES, A., PASUTTO, T., BROUTIN, L., *"Computation of Dimensionless Spectrum of Fluid Forces Induced by Vortex Shedding from a Single Rigid Tube in a Single-Phase Cross-Flow"*, in Proceedings of the 2008 International conference on Flow-Induced Vibration

[12] JUSSERAND, F., ADOBES, A., RANDRIANARIVO, T., *"Solving U-RANS k-ω SST Equations and Post-Processing Motion Independent Fluid Forces in a Tube Bundle "*, in Proceedings of the 2009 ASME PVP International Conference

[13] KAHIL, Y., BENHAMADOUCHE, S., SAGAUT, P., *"Fine Large Eddy Simulation of the Flow around One and Two Side-by-Side Infinite Cylinders at Sub-Critical Reynolds Numbers"*, V European Conference on Computational Fluid Dynamics ECCOMAS CFD 2010, PEREIRA, J., C., F., and SEQUEIRA A., eds, Lisbon, Portugal, 14–17 June 2010

[14] KRAVCHENCO, A., G., MOIN, P., *"Numerical Studies of Flow around a Circular Cylinder at Re 3900"*, Phys. Fluids. 12, pp. 403–417 (2000)

[15] LAMB, S., H., 1945, *"Hydrodynamics"*, Dover Publications, Sixth Edition

[16] LESUEUR, C., *"Rayonnement Acoustique des Structures, Vibro-Acoustique, Interactions, Fluide-Structure"*, Editions Eyrolles, Collection de la Direction des Etudes et Recherches d'Electricité de France, (1988)

[17] NAKAMURA, T., FUJITA, K., KAWANISHI, K., YAMAGUSHI, N., TSUGE, *"A Study on the Vibrating Characteristics of Tube Arrays Caused by Two-Phase Flow. Part I : Random Vibration"*, Journal of Fluids and Structures 9, pp. 519-538, (1995)

[18] NORBERG, C., *"Effects of Reynolds Number and Low-Intensity Free Stream Turbulence on the Flow round a Circular Cylinder"*, No. 87/2, Department of Applied Thermoscience and Fluid Mechanics, Chalmers University of Technology, Gothenburg, Sweden, (1987)

[19] PAPP, L., CHEN, S.S., *"Turbulence-Induced Vibration of Tube Arrays in Two-Phase Flow"*, ASME Journal of Pressure Vessel Technology 116, 312–316, (1994)

[20] PETTIGREW, M. J., TAYLOR, C. E., *"Two-Phase Flow-Induced Vibrations : an Overview"*, ASME Journal of Pressure Vessel Technology 116, 233–253, (1994)

[21] PETTIGREW, M. J., TAYLOR, C. E., *"Vibration of Tube Bundles in Two-Phase Freon Cross-Flow"*, in Flow-Induced Vibration, Vol. 273, pp. 211–226. ASME, (1994)

[22] SANDIFER, J.B., BAILEY, R.T., *"Turbulent Buffeting of Tube Arrays in Liquid Cross Flow"*, in ASME Symposium on Flow-Induced Vibrations, PAIDOUSSIS, M.P. et al. eds., (1984)

[23] SAVKAR, S.D., *"Buffeting of Cylindrical Arrays in Cross Flow"*, in ASME Symposium on Flow-Induced Vibrations, PAIDOUSSIS, M.P. et al. eds., (1984)

[24] TAYLOR, C.E., et al., *"Experimental Determination of Single and Two-Phase Cross Flow-Induced Forces on Tube Rows"*, in Flow-Induced Vibration, CHEN S.S. et al. eds., (1986)

[25] TAYLOR, C. E., PETTIGREW, M. J., AXISA, F., VILLARD, B., *"Experimental Determination of Single and Two-phase Cross Flow-Induced Forces on Tube Rows"*, ASME Journal of Pressure Vessel Technology 110, 23–28, (1988)

[26] WELCH, P., D., *"The Use of Fast Fourier Transform for the Estimation of Power Spectra : A Method Based on Time Averaging Over Short, Modified Periodograms "*, IEEE Trans. Audio Electro-acoustics Vol. AU-15, pp 70-73, (1967)